New optical tools used for characterization of phase transitions in nonlinear nano-crystals. Example of $Yb^{3+}$-doped $BaTiO_3$



2007 J. Phys.: Condens. Matter 19 096204

(http://iopscience.iop.org/0953-8984/19/9/096204)

IOP PUBLISHING JOURNAL OF PHYSICS: CONDENSED MATTER

J. Phys.: Condens. Matter **19** (2007) 096204 (14pp) doi:10.1088/0953-8984/19/9/096204

# New optical tools used for characterization of phase transitions in nonlinear nano-crystals. Example of $Yb^{3+}$-doped $BaTiO_3$

**Jaouher Amami[1], Dariusz Hreniak[2], Yannick Guyot[1], Robert Pazik[2], Wieslaw Strek[2], Christelle Goutaudier[1] and Georges Boulon[1]**

[1] Physical Chemistry of Luminescent Materials, Claude Bernard Lyon 1 University, UMR 5620 CNRS, Bâtiment Kastler, La Doua, 69622 Villeurbanne, France
[2] Institute of Low Temperature and Structure Research, Polish Academy of Sciences, Wroclaw, Poland

E-mail: georges.boulon@pcml.univ-lyon1.fr

Received 6 November 2006, in final form 15 January 2007
Published 14 February 2007
Online at stacks.iop.org/JPhysCM/19/096204

**Abstract**

The main objective of this paper is to focus on the use of new techniques to specifically characterize $BaTiO_3$ nonlinear nano-crystals as a test case. We use the second harmonic generation (SHG) of an IR YAG:Nd pump laser and detection of the $Yb^{3+}$ ion pairs to investigate effect of doping and synthesis route (sol–gel between 700 and 1200 °C) on both crystallite sizes (25–60 nm) and different phase symmetries (tetragonal, cubic, hexagonal) in $Yb^{3+}$-doped $BaTiO_3$. In nano-crystals, a higher intensity of SHG was observed in the acentric tetragonal phase, whereas the isotropic cubic phase was detected by the absence of a SHG signal. Cooperative emission, indicating the presence of $Yb^{3+}$ ion pairs, was easily detected in the cubic phase and not seen in the ferroelectric tetragonal structure.

(Some figures in this article are in colour only in the electronic version)

## 1. Introduction

Barium titanate ($BaTiO_3$) is a very well known ferroelectric perovskite material, not only for bulk crystals [1] but also for nano-crystals [2–4]. Depending on the temperature, five phases appear in bulky samples: rhombohedral, orthorhombic, tetragonal, cubic and hexagonal [5, 6]. The tetragonal phase of $BaTiO_3$, an excellent ferroelectric material, is most widely used for applications to nonlinear optics such as holographic memory storage, self-pumped conjugate mirrors and laser resonators [7–9].

The effect of grain size on the properties of $BaTiO_3$ phases is strong and manifests itself in changes of all properties: phase transition temperatures, crystal structure and nonlinear

properties [10]. The ferroelectric tetragonal phase is stable at room temperature, more precisely between 273 and 393 K. The first results on size effects were obtained by Anliker *et al* [11] in 1954. Particles in the size range 30 nm–2.3 $\mu$m were produced by ball milling. The appearance of a phase transition at the Curie temperature, $T_C$, was used as a criterion for the critical size (100–200 nm) by Yamamoto *et al* [12]. In 1993, $BaTiO_3$ powders with particle sizes between 30 and 150 nm were grown by Saegusa *et al* [13], and the phase transition at $T_C$ was detected by DSC measurements for crystallite sizes around 90 nm. Recent data on $BaTiO_3$ powders were published by Frey and Payne [14] who reported that at 1200 °C the samples were characterized by a grain size of 0.4 $\mu$m. In previous works, we also reported on the doping ion concentrations of europium and neodymium and the effects on the properties of $BaTiO_3$ nano-crystals [15, 16].

Nonlinear optical materials have a great number of applications in the performance of functions such as frequency conversion, light modulation, optical switching, optical memory storage and optical second harmonic generation (SHG), and can be used as electro-optic phase modulators to generate optical parametric frequency conversion and amplitude modulation.

In this work we report on the synthesis of $Yb^{3+}$-doped $BaTiO_3$ nano-crystals and the characterization of phase transformation behaviour by using not only classical methods such as x-ray diffraction and Raman spectroscopy but also unusual methods such as the $Yb^{3+}$ spectroscopic probe, the SHG detected only in the tetragonal phase and the cooperative effect seen with $Yb^{3+}$ pairs only in the cubic phase. Two parameters play an important role: synthesis temperature and rare earth doping ion content.

Moreover, in order to carry out a comparative study with nano-crystals, single crystals of $Yb^{3+}$-doped $BaTiO_3$ grown using the laser heated pedestal growth (LHPG) technique were investigated. Indeed, substituting barium with gadolinium [17] or neodymium [18] in $Ba_2NaNb_5O_{15}$ (BNN) reduces the thermal expansion and changes the structure between orthorhombic and tetragonal phases.

Our main objective is to focus on the use of new techniques to specifically characterize the effect of doping and synthesis route on both crystallite size and phase symmetry, using $Yb^{3+}$-doped $BaTiO_3$ nonlinear nano-crystals as a test case.

## 2. Experimental techniques

### *2.1. Synthesis of the $BaTiO_3$ nano-crystals*

Details of the preparation of $BaTiO_3$ nano-crystals were described by Hreniak *et al* [19]. Barium acetate, titanium butoxide and ytterbium oxide were used as starting materials. Acetyl acetone and acetic acid were selected as solvents of titanium butoxide and barium acetate, respectively. Ytterbium chloride was obtained by reacting stoichiometric amounts of ytterbium oxide with hydrochloric acid. Dissolved barium acetate was added dropwise to titanium butoxide solution with stirring. The obtained solutions were vigorously stirred at 50 °C for about 2 h. The ytterbium salt was dissolved in a small amount of water and added slowly to the obtained transparent yellow sol with different molar ratios of $Yb^{3+}$ versus $BaTiO_3$. The obtained sol was heated at approximately 100 °C for 24 h to form barium titanate gel. The samples of crushed gels were heated above 700 °C to form $Yb^{3+}$-doped $BaTiO_3$ nano-crystal powders. The small particles of $BaTiO_3$, grown by the sol–gel method, were characterized from Scherrer's equation from the x-ray line-widths in the size range of 25–65 nm with sintering temperature (700–1200 °C). The same procedure was used for samples prepared with different contents of $Yb^{3+}$ ions.

### *2.2. Synthesis of the $BaTiO_3$ single crystals*

Single crystal fibres were grown by the LHPG technique. The greatest advantage of this technique is the absence of a crucible, which ensures no contamination or stress [20, 21]. The ceramic feed rods were prepared from a stoichiometric mixture of the starting powders $BaCO_3$ and $TiO_2$. The $Yb^{3+}$ ion content in $BaTiO_3$ was 0, 1, 2, 3, 4, 5 and 8 at.%. The ceramic pellet, annealed three times at 1200 °C over 15 h, was then shaped into rectangular rods. The laser beam was focused on the top of the source rod to create a small molten zone where the seed rod was immersed. The growth rates were 40–50 and 10–20 mm $h^{-1}$ for the seed and the feed rod, respectively. During crystal growth, the fibres cracked perpendicularly to the growth direction. In particular, cracking occurred easily once the crystal diameter was above 0.8 mm. The obtained undoped $BaTiO_3$ fibres crystallized in the hexagonal phase as expected [6]. Incorporation of ytterbium helped to obtain rather good quality, transparent homogeneous fibres with a yellowish colour.

### *2.3. Apparatus*

Several characterizations were performed on the grown $Yb^{3+}$-doped $BaTiO_3$. Identification of the grown bulky fibre crystals and nano-crystals was performed by powder x-ray diffraction (XRD) with Ni-filtered Cu K$\alpha$ radiation, using silicon powder (99.99% purity) as an internal standard. The experimental set-up for Raman spectroscopy comprised a Dilor XY micro-Raman system with 500 nm local lengths, an Olympus microscope (50×) and a charge coupled device (CCD) detector. Excitation was provided by the 514 nm line of an argon laser.

The excitation of the $Yb^{3+}$ ion luminescence was performed by a frequency-doubled Nd:YAG laser (10 ns, 10 Hz) pumping a Quantel two-amplified-stage dye laser containing a mixture of DCM and LDS 698 and followed by a hydrogen Raman cell shifter to generate a beam in the 920–980 nm range. Detection of the near infrared luminescence was with a Jobin-Yvon JYHRS1 monochromator equipped with a 1 $\mu$m blazed grating. The signal was detected by Coast germanium and sent in a Stanford boxcar averager SRS 250. The decay kinetics was recorded with a digital Lecroy LT 342 oscilloscope. Time-resolved photoluminescence in the visible range was performed, using an intensified CCD camera coupled with an Oriel monochromator with a 400 grooves/mm grating associated with a Stanford delay generator.

## 3. Results and discussion

### *3.1. Average size and SEM micrographs*

Figure 1 illustrates the evolution of the average size of $BaTiO_3$ nano-crystal powders with heat treatment. Clearly, the grain size increased with increasing temperature. Figure 2 shows SEM photomicrographs of three of the heat treatment conditions; particularly 800, 1000 and 1200 °C. They were recorded for grain size determination for samples undergoing the transition as revealed by XRD. The samples were characterized with grain sizes of 33, 65 and 110 nm, respectively. No effect on particle size was observed when the $Yb^{3+}$ rare earth concentration was increased.

### *3.2. Structural characterization by x-ray diffraction*

Figures 3(a) and (b) show x-ray diffraction spectra of $BaTiO_3$ powders prepared at different temperatures doped with 1% $Yb^{3+}$ and those prepared at 900 °C doped with different contents of $Yb^{3+}$, respectively. Patterns were compared to the reference standard cards for the tetragonal

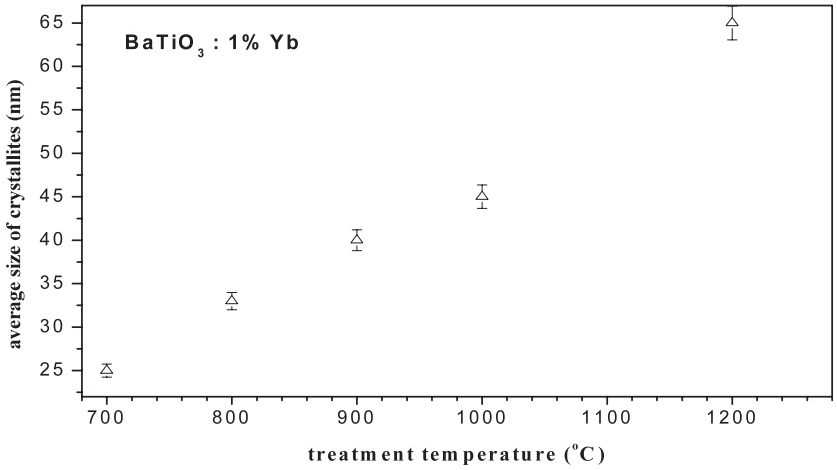


**Figure 1.** Average size of 1% $Yb^{3+}$-doped $BaTiO_3$ samples representing the room temperature cubic–tetragonal structural transition with increasing processing temperature.

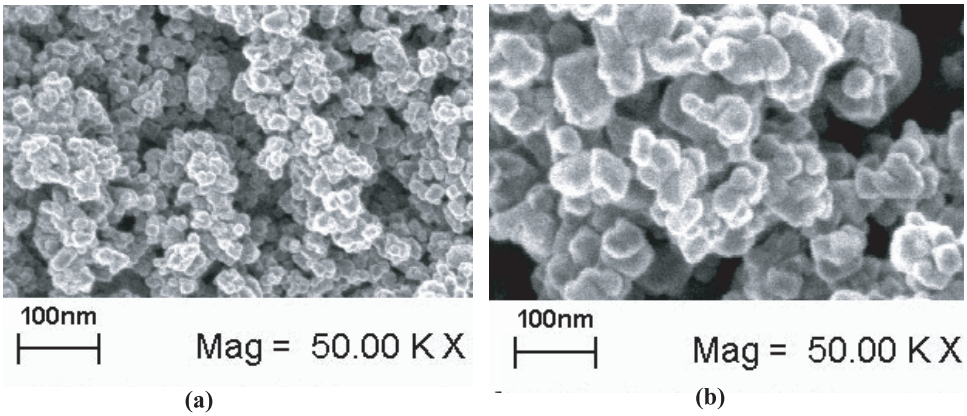


**Figure 2.** SEM photomicrographs illustrating grain growth with increasing heat treatment temperature for sintered sol–gel specimens: (a) 800 °C (33 nm) and (b) 1000 °C (50 nm).

and cubic structures of $BaTiO_3$.[3] The x-ray diffractograms of samples prepared at 1200 °C show two distinct peaks around $2\theta \approx 45.11°$ and $2\theta \approx 45.47°$ with (200 plane) and (002 plane) reflections. The same peaks appear in samples prepared at 900 °C, with a concentration of 4 at.% at $Yb^{3+}$. These peaks represent the gradual splitting of the (200 plane) reflection situated at $2\theta \approx 45.44°$, observed in 1% $Yb^{3+}$-doped $BaTiO_3$ samples prepared at 700 °C. Higher temperatures (1200 °C) are necessary to develop the net *c*-axis cell elongation normally associated with the ferroelectric transition and forming the tetragonal phase. A slight long-range lattice distortion appeared in specimens prepared at 1000 °C. Up to this temperature, the tetragonal phase was detected beside the cubic phase. Identical results were reported by Tsunkewa *et al* [22]. Takeuchi *et al* [23] looked closely at the peak positions in $2\theta \approx 45.11°$, $2\theta \approx 45.44°$ and proposed the coexistence of cubic surface layers and tetragonal grain cores.

[3] JCPDS powder diffraction file card nos 31-0174 and 05-626, respectively. International Centre for Diffraction Data, Newtome Square, PA, USA, 1967.

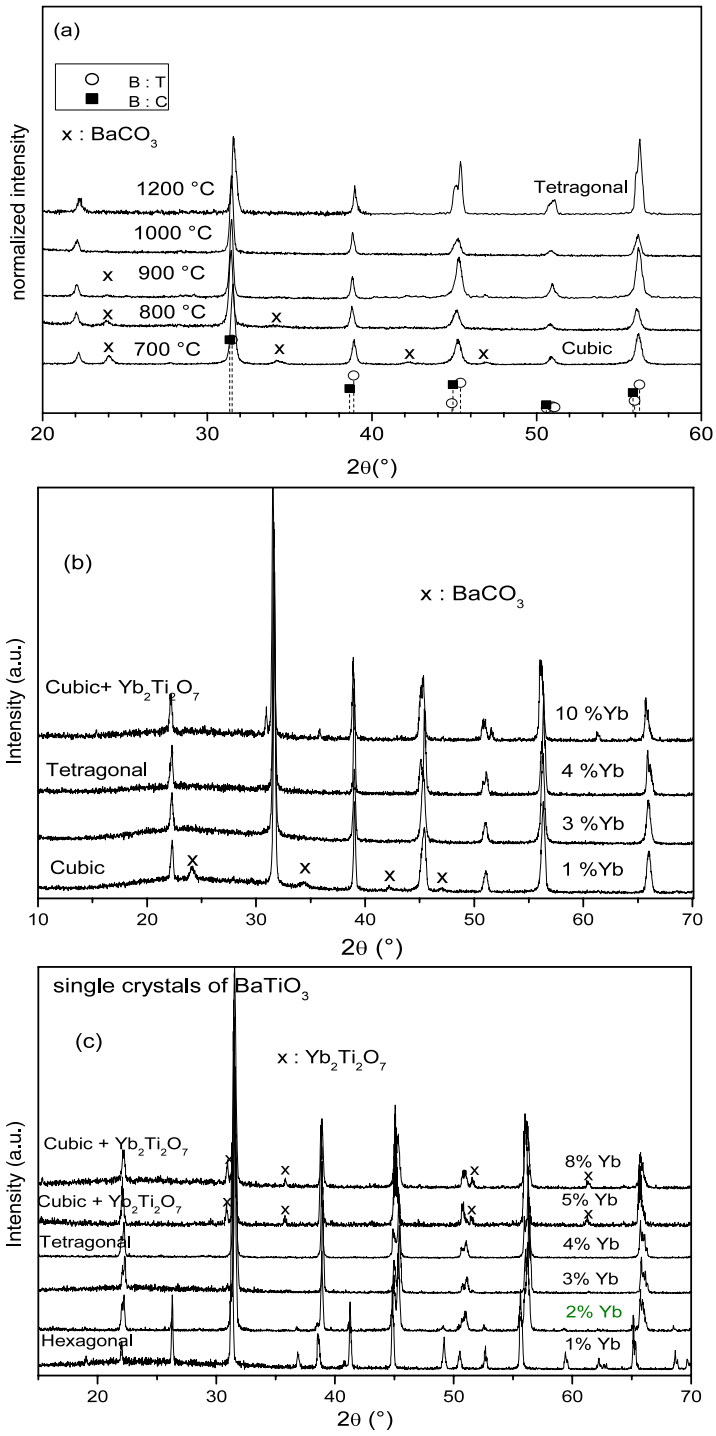


**Figure 3.** XRD patterns of (a) 1% $Yb^{3+}$-doped $BaTiO_3$ nano-crystals heated at different temperatures, (b) $BaTiO_3$ nano-crystals prepared at 900 °C and doped with different concentrations of $Yb^{3+}$ and (c) single crystal fibres of $BaTiO_3$ doped with different concentrations of $Yb^{3+}$. The scales of (a), (b) and (c) are not the same.

The cubic phase was also detected beside the tetragonal phase in the grown powders having a $Yb^{3+}$ concentration of between 2 and 3 mol% $Yb_2O_3$. These phases occur in approximately the same proportions. From the concentration of 5 at.% $Yb^{3+}$, the $Yb_2Ti_2O_7$ compound appears as a secondary phase. This ytterbium stoichiometric pyrochlore has four characteristic peaks at $2\theta = 30.9°$, 35.8°, 51.5° and 61.2°.[4] A certain amount of $BaCO_3$ was present in the samples and was stable up to at least 800 °C or when the concentration was less than 3 at.% at $Yb^{3+}$. This is represented by two high intensity peaks situated at $2\theta = 24°$ and 34° and two other weak intensity peaks at 42° and 47° [24, 25]. The presence of carbonates results from a reaction of the powder with atmospheric carbon dioxide during the conversion process. According to Wang [24] the $BaCO_3$ could also result from the slow heating rate. This result has already been reported for chemically prepared $BaTiO_3$ [26, 27].

Figure 3(c) shows powder XRD patterns of the grown single crystals of $Yb^{3+}$-doped $BaTiO_3$ recorded at room temperature. We observed a change between hexagonal (space group $P6_3/mmc$) and tetragonal (space group $P4mm$) phases occurring at a doping level between 3 and 4 at.% $Yb^{3+}$. As seen in XRD of the nano-powders, from the concentration of 5 at.% $Yb^{3+}$, the $Yb_2Ti_2O_7$ pyrochlore appeared as a secondary phase. Barium titanate crystallized in the hexagonal structure for a lower concentration of $Yb^{3+}$ (less than 1% at $Yb_2O_3$). This phase can be seen by one high intensity peak situated at $2\theta = 26.24°$. Two peaks appear at 44.97° and 45.37°, indicating the coexistence of tetragonal and hexagonal phases when 2 at.% at $Yb^{3+}$ were added. Clearly, the room temperature lattice parameter contracted when either the heat treatment temperature or the $Yb^{3+}$ rare earth doping was increased, before any global symmetry change.

Based on the XRD, the $BaTiO_3$ ferroelectric tetragonal structure was stabilized. This was made by heating nano-powders at a higher temperature (1200 °C) or by substituting $Ba^{2+}$ with about 4 at.% $Yb^{3+}$ in nano-crystals and single crystals.

### *3.3. Raman spectroscopy*

In both the paraelectric and ferroelectric phases, $BaTiO_3$ has one molecule (five atoms) per unit cell and so there are 12 optical modes. The optical modes in the paraelectric phase transform according to triply degenerate irreducible representations $3F_{1u} + 1F_{2u}$ of the $O_h$ point group. The $F_{2u}$ mode is silent and the $F_{1u}$ modes are only infrared active and so there is no Raman activity in the paraelectric $BaTiO_3$ phase with perfect cubic symmetry [28].

Figures 4(a) and (b) show spectra for the samples of $Yb^{3+}$-doped $BaTiO_3$ nano-powders prepared at different sintering temperatures or $Yb^{3+}$ doped with different ion contents, respectively. All these spectra are similar. However, contrary to XRD, Raman spectroscopy does not provide a direct structural determination.

The presence of Raman modes of high intensity in the paraelectric phase implies that this phase does not have perfect cubic symmetry but has some disorder which breaks the symmetry and permits Raman activity. As for the pseudo-cubic structure, this phase is also present for undoped barium titanate nano-powders [14]. Indeed, Raman spectroscopy is more sensitive to changes in atomic positions. All the spectra exhibit four distinct bands at 720, 515, 305 and 265 $cm^{-1}$, respectively, which are characteristic of the tetragonal phase of $BaTiO_3$ [29–31]. Referring to Perry and Hall [28], all of the peaks observed for single crystals in the tetragonal phase also appeared in the orthorhombic phase. Subtle differences in the Raman spectra between the two phases relate to features in the 180–185 $cm^{-1}$ range for powder samples.

[4] JCPDS powder diffraction file card no. 17-0454. International Centre for Diffraction Data, Newtome Square, PA, USA, 1967.

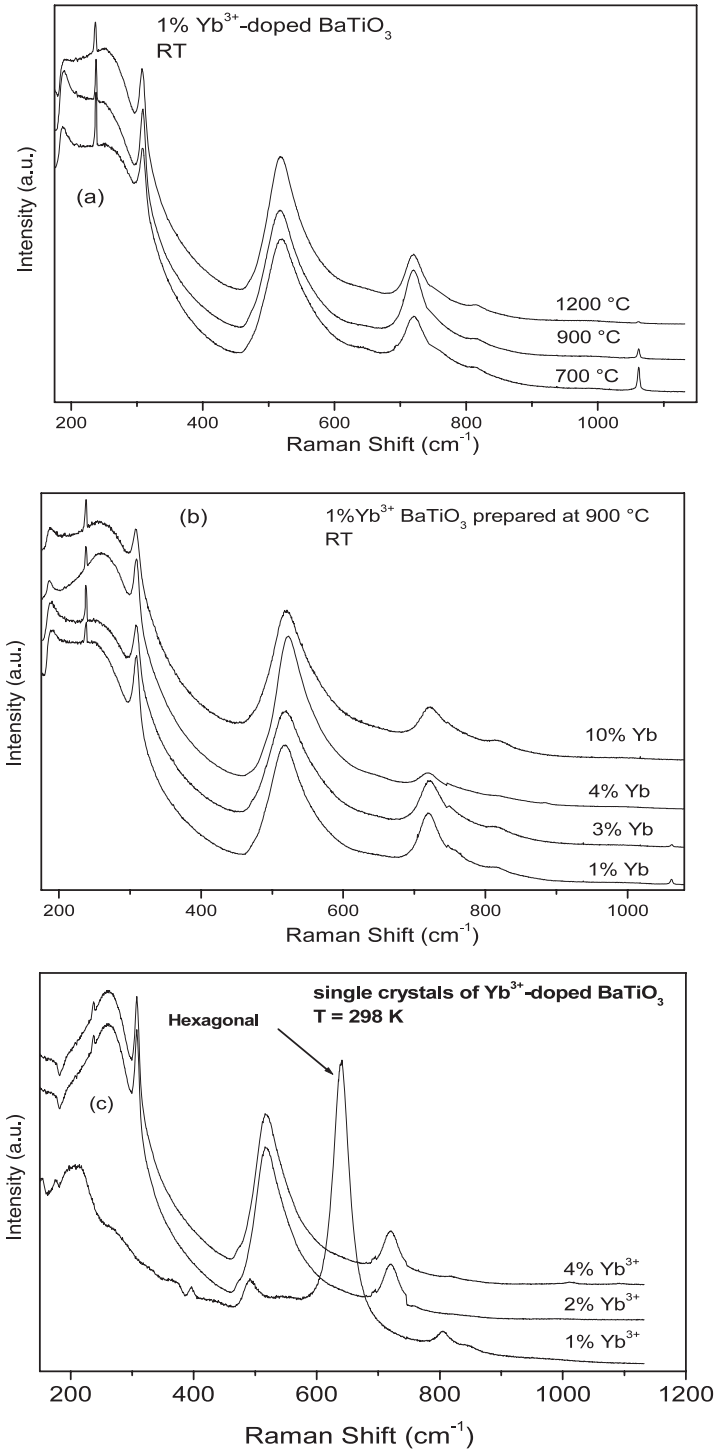


**Figure 4.** Raman spectra of (a) 1% $Yb^{3+}$-doped $BaTiO_3$ nano-crystals heated at different temperatures, (b) $BaTiO_3$ nano-crystals prepared at 900 °C and doped with different concentrations of $Yb^{3+}$ and (c) single crystal fibres of $BaTiO_3$ doped with different concentrations of $Yb^{3+}$.

A common fact in all of the Raman spectra is the presence of a peak at 1062 $cm^{-1}$. This peak whose frequency remains constant with increasing temperature is related to the carbonate ions [32]. Such a carbonate phase Raman band was not completely eliminated until the calcination temperature was raised above 1200 °C. We also observed a feature at 818 $cm^{-1}$ which corresponded to amorphous $BaTiO_3$ with a distorted molecular structure [33].

Studies of the $Yb^{3+}$ rare earth effect and the temperature effect by Raman spectroscopy did not show any phase transition change in $Yb^{3+}$-doped $BaTiO_3$ nano-powders. Therefore, the Raman study of the single crystals was an important factor in determining the difference between tetragonal and hexagonal structures in figure 4(c). The spectrum of 1% $Yb^{3+}$-doped $BaTiO_3$ revealed the presence of one distinct peak situated at 640 $cm^{-1}$. This peak was never observed in the other $BaTiO_3$ structures and is characteristic of the hexagonal phase [30]. Raman spectroscopy was not a powerful enough technique to easily distinguish between different phase transitions of $BaTiO_3$. Therefore, the second harmonic generation (SHG) and $Yb^{3+}$ cooperative emission were used as structural probes for different phase transitions in both $BaTiO_3$ nano-powders and in single crystals.

### *3.4. Characterization by $Yb^{3+}$ probe IR emission properties*

Single $Yb^{3+}$ ions have only two stark-split energy manifolds, the ground state $^2F_{7/2}$ and the excited state $^2F_{5/2}$ at around 10 000 $cm^{-1}$. Stark levels are distributed in the two manifolds and labelled from 1 to 4 in the ground state and from 5 to 7 in the excited state from the lowest to the highest energy as can be seen in the inset of figure 5(a). An important parameter is the position of the resonant zero-phonon line mentioned as $1 \leftrightarrow 5$ in figure 5(a).

*3.4.1. Sintering temperature dependence.* The emission spectra of the samples of $BaTiO_3$ prepared at different temperatures and doped with different $Yb^{3+}$ contents are plotted in figure 5. These spectra, recorded at 12 K under nonselective excitation around 960 nm, were completely different and clearly show two distinct structures which were assigned to cubic and tetragonal phases by analogy with x-ray spectra. Several bands corresponding to both the electronic and vibronic transitions complicated the total assignment of $Yb^{3+}$ energy levels in $BaTiO_3$.

- The resonant electronic transition, the so-called zero-phonon line ($5 \rightarrow 1$), was clearly detected at 981 nm in the samples prepared at 700 °C with the cubic phase and shifted to 977 nm for those sintered at 1200 °C corresponding to the ferroelectric tetragonal phase.
- Three other peaks at higher energy, situated around 985, 993 and 998 nm, belonged to the cubic structure. These peaks disappeared in the samples prepared at higher temperature (1200 °C).

In order to assign the vibronic contribution and zero-phonon electronic transition, we reported Raman spectra (R) investigated at room temperature and emission spectra (E) recorded at 12 K in figure 6. The two spectra were adjusted to the same energy scales, the origin being taken at the zero-line energy position.

For the samples prepared at a higher temperature (1200 °C) and crystallizing in the tetragonal structure we observed two intense peaks in the emission spectrum situated at 1006 and 1029 nm and coinciding with the tetragonal Raman lines at 305 and 720 $cm^{-1}$ respectively. These peaks have a broad structure and can mask the presence of vibronic activity. This phase was characterized by two other peaks situated at 1014 and 1020 nm. Formation of the ferroelectric structure was seen from 900 °C with the appearance of the characteristic weak peak at 977 nm. The peaks around 1029 and 1042 nm were observed in both cubic and tetragonal

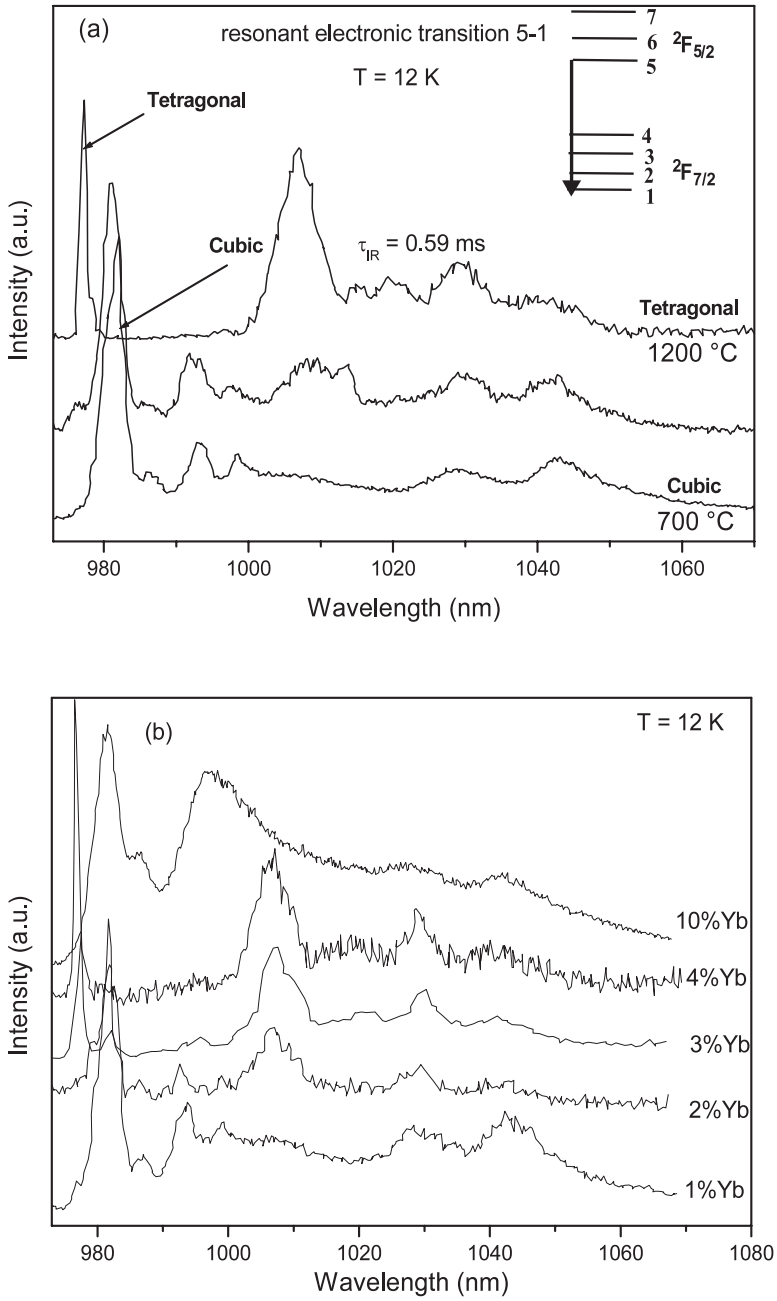


**Figure 5.** IR emission spectra, recorded at 12 K, of (a) 1% $Yb^{3+}$-doped $BaTiO_3$ nano-crystals heated at different temperatures and (b) $BaTiO_3$ nano-crystals prepared at 900 °C and doped with different concentrations of $Yb^{3+}$.

structures but with different proportions. The peak situated at 1042 nm was dominant in the paraelectric cubic phase and the peak situated at 1029 nm was dominant in the ferroelectric tetragonal structure.

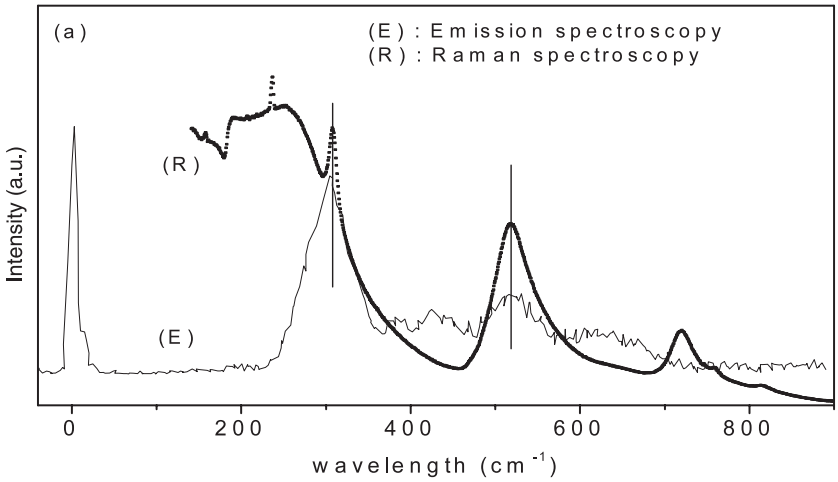


**Figure 6.** Interpretation of vibronic transitions in tetragonal $Yb^{3+}$-doped $BaTiO_3$ nano-crystals with the help of the IR emission spectrum and the Raman spectrum.

*3.4.2. $Yb^{3+}$ concentration dependence.* The assignment of pure electronic transitions of $Yb^{3+}$ ions is relatively difficult. This is due to the strong interaction of $Yb^{3+}$ ions with the lattice vibrations. These effects can give rise to strong vibronic bands or to the deformation or splitting of electronic lines in the case of resonant coupling which significantly complicates the spectra [34]. Figure 5(b) shows the emission spectra of $BaTiO_3$ prepared at 900 °C and doped with different concentrations of $Yb^{3+}$ ions. The samples doped with 2 and 3 mol% $Yb_2O_3$ crystallizing in the cubic phase exhibited the same spectra. The zero-phonon line seen by the $5 \rightarrow 1$ transition was situated at about 982 nm. When 3 at.% at $Yb^{3+}$ was added, the intensity of this peak decreased and the resonant electronic transition appeared at about 978 nm, indicating the formation of the tetragonal phase with few traces of cubic structure. Consequently, $BaTiO_3$ had a single ferroelectric tetragonal phase at 4% $Yb^{3+}$ with the zero-phonon emission peak situated at 977 nm. At 10 mol% in $Yb_2O_3$, the emission spectrum was different due to the second phase of $Yb_2Ti_2O_7$ pyrochlore which is characterized by the zero-phonon peak at 982 nm indicating coexistence with the cubic phase. The same result was found above in the x-ray diffraction part.

### *3.5. Second harmonic generation (SHG) signal and cooperative fluorescence in $Yb^{3+}$-doped $BaTiO_3$*

The capability of generating the second harmonic and the $Yb^{3+}$ cooperative fluorescence for both nano-powders and single crystals of $Yb^{3+}$-doped $BaTiO_3$ is shown in figure 7.

*3.5.1. Second harmonic generation (SHG) in $BaTiO_3$.* Crystals capable of generating the second harmonic must have a unit cell with no centre of inversion, and this requirement is met by few phases of $BaTiO_3$. Measurements of the second harmonic generation (SHG) signal intensity provide information related to the magnitude of acentric distortions for ultra-fine materials. That is, the nonlinear optical behaviour of tetragonal $BaTiO_3$ varies with the grain size [14].

In figure 7(a) we can see SHG of either a 938 or 976 nm IR excitation pump laser recorded at room temperature for all samples of $Yb^{3+}$-doped $BaTiO_3$. The agreement of the

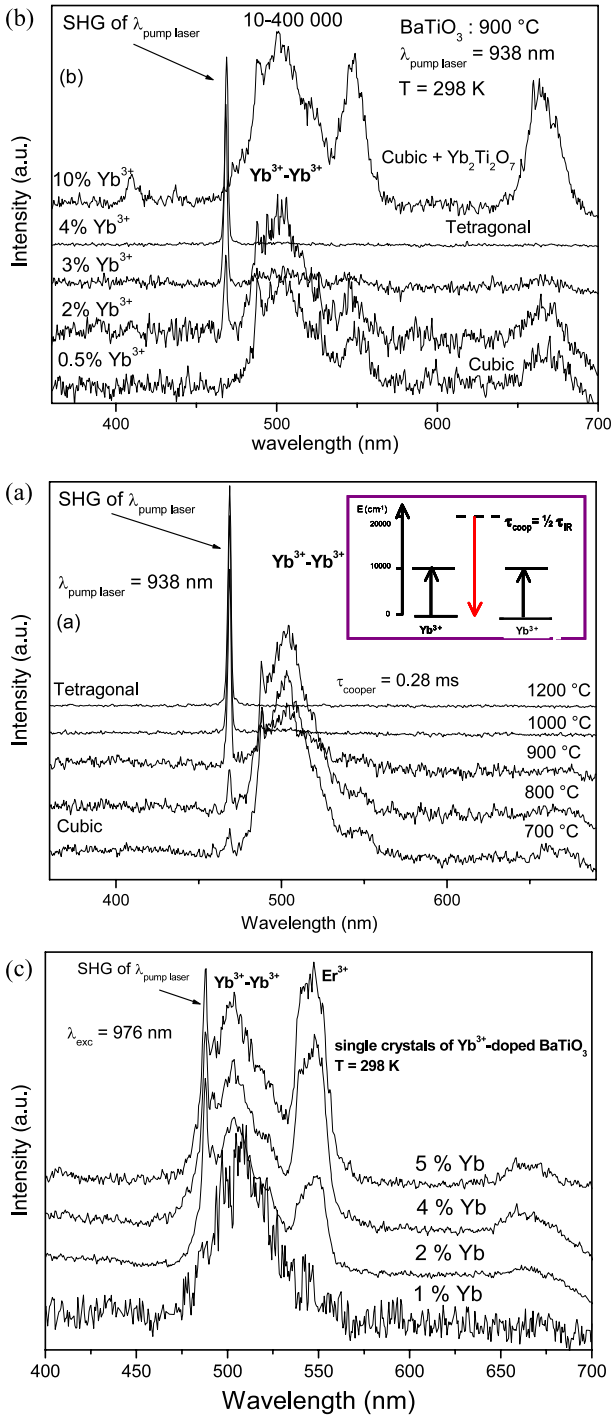


**Figure 7.** SHG signal, up-conversion emission spectrum of rare earth impurities under $Yb^{3+}$ pumping in the IR and visible cooperative emission spectrum of $Yb^{3+}$ ion pairs at room temperature of (a) 1% $Yb^{3+}$-doped $BaTiO_3$ nano-crystals heated at different temperatures, (b) $BaTiO_3$ nano-crystals prepared at 900 °C and doped with different concentrations of $Yb^{3+}$ and (c) single crystal fibres of $BaTiO_3$ doped with different concentrations of $Yb^{3+}$.

two SHG signals in the visible at half-wavelength of the two IR excitation wavelengths (469 and 488 nm, respectively) favours the real probe of the nonlinear effect in nano-crystal powders. A significant enhancement in the intensity of the SHG signal was observed in samples heated at higher temperatures (>1000 °C) and in those doped at 4% in $Yb_2O_3$. All these samples crystallized in the anisotropic tetragonal structure. Such an increase in the SHG signal intensity was due to phase transition from the isotropic cubic phase to the tetragonal one which is characterized by a lower symmetry.

The pyrochlore ytterbium oxide described by the chemical formula $Yb_2Ti_2O_7$ has a face-centred cubic crystal structure with a strong crystal field in the isotropic space group $Fd3m$. Therefore, $Yb_2Ti_2O_7$ was detected by the absence of the SHG signal.

All the single crystals, except the sample doped with 1% $Yb^{3+}$ crystallizing in the hexagonal structure, presented a high intensity SHG signal at half-wavelength (488 nm) of the IR laser excitation (976 nm). Concerning the 1% $Yb^{3+}$-doped $BaTiO_3$ single crystal sample crystallizing in the hexagonal phase, only a very weak intensity SHG signal was observed. In the literature, Filippetti and Hill reported [35] that the $BaTiO_3$ hexagonal phase displays both magnetic and ferroelectric properties.

*3.5.2. Cooperative emission of $Yb^{3+}$ pair ions.* Cooperative emission is a simultaneous radiative relaxation of excited $Yb^{3+}$ pair ions. The signature is given as the convolution of the IR emission spectrum of $Yb^{3+}$ isolated ions. The signal can be seen around 500 nm as in other $Yb^{3+}$-doped oxides we have already studied [36].

The highest intensity of the cooperative emission corresponds to the samples prepared at the lowest temperature (700 °C) and to samples doped with less than 2 at.% $Yb^{3+}$ in the cubic structure. Indeed, this signal was not seen at temperatures above 1000 °C and for samples doped with 3–4 at.% $Yb^{3+}$. This can be explained by the disorder in the paraelectric cubic phase which is associated with the position of the Ti atoms. Instead of occupying the centre positions as in a perfect cubic perovskite structure, the Ti atoms are thought to be displaced along the cube diagonals causing the disorder [37], and then pairs of $Yb^{3+}$ are easily formed as clusters. In the tetragonal phase, however, the symmetry is perfect and no structural distortion has been reported in the literature. Therefore, $Yb^{3+}$ ions are better substituted and placed in the structure. Another explanation can be given: the absence of pairs in the tetragonal phase can be related to the overlapping of the orbitals. In fact, in $BaTiO_3$ there is a certain amount of hybridization between d(Ti) and p(O) charge causing a fraction of d(Ti) states to be occupied. The d(Ti) has two contributions coming from the $t_{2g}$ triplet and the $e_g$ doublet of orbitals and both $e_g$ and $t_{2g}$ states are hybridized with the p(O)-type manifold. The breaking of cubic symmetry splits the $t_{2g}$ orbitals into one singlet ($dxy$) and one doublet ($dxz$ and $dyz$), and the $e_g$ orbital into two singlets. So, there is an overlapping of orbitals by p–d hybridization in $BaTiO_3$ [35]. A higher intensity of pairs was observed in 10% $Yb^{3+}$. This can be explained by considering that in nano-crystal oxides the probability of forming ion pairs increases with increase in the rare earth doping content.

In fact, ion pairs and even clusters are easily formed in the $BaTiO_3$ lattice, replacing $Ba^{2+}$ or $Ti^{4+}$ sites. There were two stages of substitution of rare earth elements in $BaTiO_3$. In the first stage, $Ti^{4+}$ ions located on the B site were replaced by rare earth elements. In the second stage $Ba^{2+}$ ions on the A site were also mainly replaced by rare earth elements [38]. $Yb^{3+}$ ions (0.98 Å) most probably replaced $Ba^{2+}$ (1.56 Å in radius) cations rather than $Ti^{4+}$ (0.65 Å), whose radius seems too small. When $Yb^{3+}$ was introduced to $BaTiO_3$, three $Ba^{2+}$ sites were substituted by two $Yb^{3+}$ neighbours to keep electrical neutrality and so one vacancy was created. The substitution of both $Ti^{4+}$ and $Ba^{2+}$ was also possible, but less probable. The crystal chemistry of $BaTiO_3$ could be altered to retain the local charge balance.

Figure 7(c) shows the spectra of the cooperative fluorescence and the SHG signal of $Yb^{3+}$-doped $BaTiO_3$ single crystals. All of them presented the same broad band around 503 nm indicating the $Yb^{3+}$ ion pairs. The fluorescence intensity decreased slightly with the $Yb^{3+}$ concentration. Contrary to nano-crystals, the pairs in single crystals were observed in the tetragonal phase. In fact, fibres grown by the LHPG technique were characterized by aggregates which were able to alter the structure. In previous works on $Yb^{3+}$-doped crystals, we showed that the LHPG technique favoured the formation of pairs compared to crystals grown by the Czochralski technique [39].

## 4. Conclusion

Nano-crystals of sol–gel powders of sizes ranging from 25–65 nm and single crystal fibres of $Yb^{3+}$-doped $BaTiO_3$ grown by the LHPG technique, were synthesized. X-ray diffraction and Raman spectroscopy were used as standard techniques to probe cubic, tetragonal and hexagonal phases. In addition, $Yb^{3+}$ IR emission spectroscopy under laser excitation, SHG of the IR pumped laser and cooperative emission from $Yb^{3+}$ ion pairs were used as unusual optical methods to probe phase transitions. Data suggest that an enhanced stability exists for the tetragonal structure when the grain size increases above 45 nm for temperatures greater than 1000 °C and when 3–4 at.% $Yb^{3+}$ is added for both nano-crystals and single crystals of $BaTiO_3$. The centrosymmetric cubic samples did not exhibit any SHG. Cooperative emission, indicating pairs of $Yb^{3+}$ ions in nano-crystals, were easily detected in the cubic and hexagonal phases but were not seen in the ferroelectric tetragonal structure. Consequently, our main objective was to focus on the use of these new techniques to specifically characterize the effect of doping and synthesis route on both crystallite sizes and phase symmetries using $Yb^{3+}$-doped $BaTiO_3$ nonlinear nano-crystals as a test case.

## Acknowledgments

This work was supported by CNRS and especially under CNRS-Polish Academy of Sciences Associated Project for 4 years. These studies were also partially supported by the Polish Ministry of Science under Grant No. 3 T08A 006 29. The authors are grateful to Dr Dmitrij Kolesnikov IHPP Warsaw for the SEM measurements.

## References

[1] Megaw H D 1945 *Nature* **155** 484
[2] Alinker M, Brugger H R and Kanzig T 1954 *Helv. Phys. Acta* **27** 99
[3] Shaikh A, Vest R and Vest G 1990 *IEEE Trans. Ultrason. Ferroelectr. Freq. Control* **36** 407
[4] Muller J U and Barner K 1990 *Ferroelectr. Cryst.* **108** 83
[5] Jona F and Shirane G 1962 *Ferroelectric Crystals* (London: Pergamon)
[6] Rase D E and Roy R 1955 *J. Chem. Phys.* **38** 102
[7] Townsend R L and LaMacchia J T 1970 *J. Appl. Phys.* **41** 5188
[8] Feinberg J and Hellwarth R W 1980 *Opt. Lett.* **5** 519
[9] Feinberg J 1982 *Opt. Lett.* **7** 486
[10] Setter N and Waser R 2000 *Acta Mater.* **48** 151
[11] Anliker M, Brugger H R and Kaenzig W 1954 *Helv. Phys. Acta* **27** 99
[12] Yamamoto T, Urabe K and Banno H 1993 *Japan. J. Appl. Phys.* **32** 4272
[13] Saeguna K, Wendell E R and Bowen H K 1993 *J. Am. Ceram. Soc.* **76** 1505
[14] Frey M H and Payne D A 1996 *Phys. Rev.* B **54** 3158
[15] Stręk W, Hreniak D, Boulon G, Guyot Y and Pązik R 2003 *Opt. Mater.* **24** 15
[16] Pązik R, Hreniak D and Stręk W 2007 *Mater. Sci.* **22** 219

[17] Shimazu W, Tsukioka M, Mitoke N, Kuroiwa S and Tsutsumi S 1990 *J. Mater. Sci.* **25** 4525
[18] Foulon G, Ferriol M, Brenier A, Cohen-Adad M-T, Boudeulle M and Boulon G 1997 *Opt. Mater.* **8** 65
[19] Hreniak D, Łukowiak E, Maruszewski K, Pązik R and Stręk W 2002 *Mater. Sci.* **20** 43
[20] Feigelson R S 1985 *Spinger Ser. Opt. Sci.* **47** 129
[21] Goutaudier C, Lebbou K, Guyot Y, Ito M, Canibano H, El Hassouni A, Laversenne L and Boulon G 2003 *Ann. Chim. Sci. Mater.* **28/6** 73
[22] Tsunkawa S, Ito S, Mori T, Ishikawa K, Li Z and Kawazoe Y 2000 *Phys. Rev.* B **62** 3065
[23] Takeuchi T, Ado K, Asai T, Kageyama H, Saito Y, Masquelier C and Nakamura O 1994 *J. Am. Ceram. Soc.* **77** 1665
[24] Takeuchi T, Tabuchi M, Ado K, Nakamura O, Kageyama H, Suyama Y, Ohtori N and Nagazawa M 1997 *J. Mater. Sci.* **32** 4053
[25] Wang H W 2002 *Mater. Chem. Phys.* **74** 1
[26] Naka S, Nakakita F, Suwa Y and Inagaki M 1974 *Bull. Chem. Soc. Japan* **47** 1168
[27] Uchino K, Sadanaga E and Hirose T 1989 *J. Am. Ceram. Soc.* **72** 1555
[28] Perry C H and Hall D B 1965 *Phys. Rev. Lett.* **15** 700
[29] Zhang H X, Kam C H, Zhou Y, Han X Q, Lam Y L, Chan Y C and Pita K 2000 *Mater. Chem. Phys.* **63** 174
[30] Preda L, Courselle L, Despax B, Bandet J and Ianculescu A 2001 *Thin Solid Films* **389** 43
[31] Kim Y-I, Jung K-J and Ryu K-S 2001 *Mater. Res. Bull.* **95** 1
[32] Duran P, Capel F, Tartaj J, Gutierrez D and Moure C 2001 *Solid State Ion.* **141/142** 529
[33] Gottmann J, Vosseler B and Kreutz E W 2002 *Appl. Surf. Sci.* **197/198** 831
[34] Ellens A, Andres H, Meijerink A and Blasse G 1997 *Phys. Rev.* B **55** 173
[35] Filippetti A and Hill N A 2002 *Phys. Rev.* B **65** 2264
[36] Guyot Y, Canibano H, Goutaudier C, Novoselov A, Yoshikawa A, Fukuda T and Boulon G 2005 *Opt. Mater.* **27** 1658
Guyot Y, Canibano H, Goutaudier C, Novoselov A, Yoshikawa A, Fukuda T and Boulon G 2006 *Opt. Mater.* **28** 1
[37] Comes R and Lambert M 1969 *Solid State Commun.* **7** 305
[38] Watanabe K, Ohsato H and Kishi H 1998 *Solid Ion. State* **108** 129
[39] Bensalah A, Guyot Y, Brenier A, Sato H, Fukuda T and Boulon G 2004 *J. Alloys Compounds* **380** 15